

Active buckling of pressurized spherical shells : Monte Carlo Simulation

Vipin Agrawal,^{1,2,*} Vikash Pandey,^{1,†} and Dhrubaditya Mitra^{1,‡}

¹*Nordita, KTH Royal Institute of Technology and Stockholm University, Roslagstullsbacken 23, 10691 Stockholm, Sweden*

²*Department of Physics, Stockholm university, Stockholm, Sweden.*

(Dated: February 23, 2023)

We study the buckling of pressurized spherical shells by Monte Carlo simulations in which the detailed balance is explicitly broken – thereby driving the shell active, out of thermal equilibrium. Such a shell typically has either higher (active) or lower (sedate) fluctuations compared to one in thermal equilibrium depending on how the detailed balance is broken. We show that, for the same set of elastic parameters, a shell that is not buckled in thermal equilibrium can be buckled if turned active. Similarly a shell that is buckled in thermal equilibrium can unbuckle if sedated. Based on this result, we suggest that it is possible to experimentally design microscopic elastic shells whose buckling can be optically controlled.

Thin spherical shells are commonly found in many natural and engineering settings. Their sizes can vary over a very large range – from hundred meters, e.g., the Avicii Arena Stockholm [1] down to about hundred nanometers, e.g., viral capsules [2, 3] and exosomes [4, 5]. The elastic properties of shells, including conditions under which buckling can occur, have been extensively studied [6–11]. Interest in this traditional field of applied mathematics has been rekindled in the past decades because of possible applications to biology and nanoscience [2, 3, 12–20]. For example, the elastic shell is used as model for nuclear membrane [21]. Furthermore, the cell membrane, although often modeled simply as a fluid membrane, is dynamically tethered to the cytoskeleton – thereby acquiring effective in-plane elastic properties. For example, it has been shown [22] that to capture the stomatocyte–discocyte–echinocyte sequence of the human red blood cell within one unified model it is necessary to introduce nonlinear in-plane shear elastic modulus of the membrane. Numerical simulations of flowing RBCs that faithfully reproduce experimental observations also must use nonlinear shear elastic modulus [23, 24, 26–29]. Crucially, it has been shown that for small enough shells the thermal fluctuations can bring down the critical buckling pressure by a large amount [30, 31]. This opens up the intriguing possibility of how the elastic properties of shells, in particular buckling, will change if they are turned active – driven out of thermal equilibrium. The fundamental property of living matter is that they are not in thermal equilibrium [32] even when they are statistically stationary. They are active – they consume energy and generate entropy [33]. The statistical and mechanical properties of active matter is a current topic of considerable interest [34, 35]. The fluctuations of the membrane of living cells have active components, in addition to the thermal fluctuations, due to, e.g., driving by the active cytoskele-

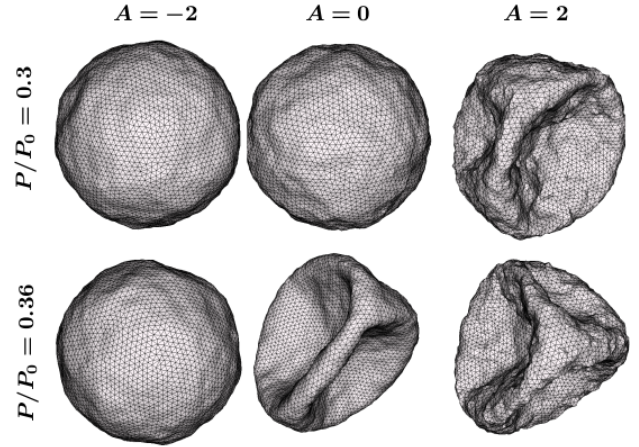


FIG. 1. Active buckling: Typical snapshots from our simulations for activity $A = -2, 0$ and 2 (from left to right), and pressure $P = 0.30P_0$ (top row) and $0.36P_0$ (bottom row) where P_0 is the critical buckling pressure obtained from the mechanical theory of elastic shells, i.e., at zero temperature. We use $N = 5120$, $FvK = 4616$, and $ET = 8$. The middle column, $A = 0$, corresponds to shells in thermal equilibrium – an unbuckled shell buckles upon increasing P/P_0 from 0.30 to 0.36 . This is consistent with the results of Refs. [30, 31]. Top row: As activity is increased to 2 (right column) the shell buckles. Bottom row: Whereas as activity is decreased to -2 (left column) the shell, that was buckled in thermal equilibrium, does not buckle at the same pressure.

ton [36–40]. Active shells can also be synthetically designed, e.g., by embedding certain proteins, who acts as active pumps when irradiated with light of certain frequency, in bi-lipid membranes [41, 42]. Shells made out of hard-magnetic elastomers can be turned active by an external magnetic field [43].

In this paper, we study the buckling of pressurized active spherical shells using the Monte Carlo (MC) simulations [44] in which detailed balance is explicitly broken – thereby driving the shell active, out of thermal equilibrium. Such a shell typically has either higher or lower

* vipin.agrawal@su.se

† vikash.pandey@su.se

‡ dhruba.mitra@gmail.com

fluctuations than thermal ones depending on how the detailed balance is broken. We call such non-equilibrium stationary states *active* and *sedate* respectively. We show that, within the right range of elastic parameters, a shell that is not buckled in thermal equilibrium can be buckled if turned active. Similarly a shell that is buckled in thermal equilibrium can unbuckle if turned sedate, see Fig. (1). Based on our study, we suggest that it is possible to experimentally design microscopic elastic shells whose buckling can be optically controlled.

Let us briefly summarize, following Refs. [30, 31] the model and the key results of theory of thin elastic shells in *thermal equilibrium*. A pressurized elastic shell is described by an effective Hamiltonian, $G_{\text{eff}} = G_0 + G_1$ where,

$$G_0[f] = \frac{1}{2} \int d^2\mathbf{x} \left[B(\nabla^2 f)^2 - \frac{PR}{2} |\nabla f|^2 + \frac{Y}{R^2} f^2 \right], \text{ and} \quad (1a)$$

$$G_1[f] = \frac{Y}{2} \int d^2\mathbf{x} \left[\left(\frac{1}{2} \mathcal{P}_{ij} \partial_i f \partial_j f \right)^2 - \frac{f}{R} \mathcal{P}_{ij} \partial_i f \partial_j f \right]. \quad (1b)$$

Here $\mathbf{x} = (x_1, x_2)$ is a two-dimensional Cartesian coordinate system and $\mathcal{P}_{ij} \equiv \delta_{ij} - \partial_i \partial_j / \nabla^2$ is the transverse projection operator. The out-of-plane displacement is $h(\mathbf{x}) = f_0(\mathbf{x}) + f(\mathbf{x})$ where $f_0(\mathbf{x})$ is the uniform contraction of the sphere in response to the external pressure. The difference between the external and the internal pressure is P . The part G_0 is harmonic and the part G_1 is anharmonic. In this model, we assume the shell to be amorphous and homogeneous with radius R , bending modulus B and (two-dimensional) Young's modulus Y . Two non-dimensional numbers determine the elastic behavior of such shells, the Föppl-von-Karman number and the Elasto-thermal number, defined respectively as

$$\text{FvK} \equiv \frac{Y R^2}{B}, \quad \text{ET} \equiv \frac{k_B T}{B} \sqrt{\text{FvK}}, \quad (2)$$

where k_B is the Boltzmann constant and T is temperature. At constant ET, the effects of anharmonicity increases with FvK whereas at constant elastic moduli the effects of thermal fluctuations increases with ET. Ignoring the anharmonic contribution, using standard tools of equilibrium statistical mechanics it is straightforward [30, Eq. 4] to calculate the spectrum of fluctuations

$$S(\mathbf{q}) \equiv \langle \hat{f}(\mathbf{q}) \hat{f}(-\mathbf{q}) \rangle = \frac{k_B T}{a \left(B q^4 - \frac{P R q^2}{2} + \frac{Y}{R^2} \right)}, \quad (3)$$

where $\hat{f}(\mathbf{q})$ is the Fourier transform of $f(\mathbf{x})$ and a is the area of integration in the (x_1, x_2) plane. In equilibrium, the symbol $\langle \cdot \rangle$ denotes thermal averaging; whereas for active cases, it denotes averaging over the non-equilibrium

stationary states. Note that $S(\mathbf{q})$ blows-up for

$$P = P_0 \equiv \frac{4B}{R} q_*^2, \quad \text{where} \quad (4a)$$

$$q_* \equiv \left(\frac{Y}{B R^2} \right)^{1/4} = \frac{\text{FvK}^{1/4}}{R}, \quad (4b)$$

where P_0 is the buckling pressure, independent of temperature, obtained within the traditional theory [11] of buckling of pressurized shells. For a large Föppl-von-Karman number, $q_* > 1/R$ is the buckling mode. Refs. [30, 31] used renormalization group (RG) techniques to show that the effects of the anharmonic terms is to renormalize the parameters appearing in the bare theory, i.e., P , B , and Y in (3) must be replaced by their scale-dependent, renormalized versions, see Ref. [31, Eq. 18]. Consequently both the pressure and the critical buckling pressure are renormalized and buckling is obtained if both of these quantities are equal for a length scale which must be smaller than the radius of the sphere [31]. The results of this RG analysis were validated by Monte Carlo simulations of spherical shell, randomly triangulated with N grid points, with discretized bending and stretching energies that translate directly into a macroscopic elastic moduli [30, 45, 47]. Our Monte Carlo code, described in detail in Ref. [48], closely follows that of Ref. [30], and faithfully reproduces these results. We incorporate activity into this model in the following manner.

Over the years, many theoretical models [49–55], have been suggested to incorporate the effects of active fluctuations into models of membranes. We use a method that is well suited to use the Monte Carlo setup and has been used before to study Ising models out of equilibrium [44, 56–58] – the idea is to break detailed balance while preserving stationarity. In equilibrium Monte Carlo simulations two common choices of the transition rate from one state to another are the Metropolis (W_{Met}) and the Glauber (W_{Gla}), given respectively by,

$$W_{\text{Met}} = \min \left[1, \exp \left(-\frac{E}{k_B T} \right) \right], \text{ and} \quad (5a)$$

$$W_{\text{Gla}} = \frac{1}{2} \left[1 - \tanh \left(\frac{E}{2 k_B T} \right) \right], \quad (5b)$$

where k_B is the Boltzmann constant, T is the temperature and E is the difference in energy between the two states. To drive the membrane out of equilibrium, following Ref. [44], we replace E by $E + \Delta E$ where ΔE is a constant. This guarantees that detailed balance is broken and the amount by which it is broken is ΔE . If ΔE is positive (negative) the probability of acceptance of large fluctuations is decreased (increased). Thus we define a dimensionless quantity $A = -\Delta E / (k_B T)$ such that simulations with positive A , *active* simulations, have higher fluctuations than equilibrium ones whereas for negative A , *sedate* simulations, the fluctuations are less than the equilibrium ones. For most of the simulations reported here we use the Metropolis algorithm. In some representative cases, for both equilibrium and non-equilibrium

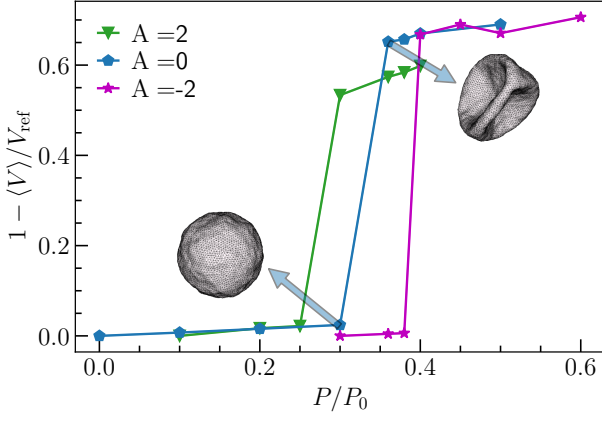


FIG. 2. **Buckling under pressure:** Normalized change in volume as a function of external pressure for (blue) a shell in thermal equilibrium, (green) active ($A = 2$), and (magenta) sedate ($A = -2$) for simulations with $ET = 8$ and $FvK = 4616$ and number of grid points $N = 5120$. Here $\langle V \rangle$ is the ensemble average of volume, and V_{ref} is the average volume at the smallest pressure difference. The error in $\langle V \rangle$ are the shades around the solid lines – they are too small to be visible. The signature of buckling is the sudden large change in volume. The critical buckling pressure for the thermal case is consistent with Refs [30, 31].

simulations, we have checked that both the Glauber and Metropolis algorithm gives the same result.

For lipid vesicles in thermal equilibrium, standard techniques of equilibrium statistical mechanics [39] and micropipet aspiration experiments show $\Delta\alpha \propto (k_B T / 4\pi B) \ln \sigma$ where $\Delta\alpha$ is the areal strain and σ is the surface tension. For active membranes the same proportionality holds but the constant of proportionality is different [42]. This experimental result was captured by the model in Ref. [59] which adds an additional Ornstein–Uhlenbeck noise to the models of thermal membranes. Our active Monte Carlo scheme, in planar membranes [60] reproduces the results of, Ref. [59] and also the experimental result of Ref. [42].

In summary, we incorporate the technique of active Monte Carlo [44] into the Monte Carlo algorithm for spherical shells in thermal equilibrium [30, 45, 48] to simulate active shells.

In Fig. (2) we show a typical plot of how the volume, V , of the spherical shell changes as the external pressure is increased from a very small value. The simulations are done in a constant pressure ensemble, hence volume is a fluctuating quantity. Henceforth, by volume we mean the average volume $\langle V \rangle$. The average volume at the smallest pressure difference, is the reference volume V_{ref} . The error in $\langle V \rangle$, shown by the shaded regions in Fig. (2) are the variances – they are too minute to be visible. First consider the shell under thermal equilibrium. Buckling shows up as a sharp decrease in volume accompanied by a typical buckled shape, as shown in Fig. (1). The critical buckling pressure, P_c , that we obtain is consistent with

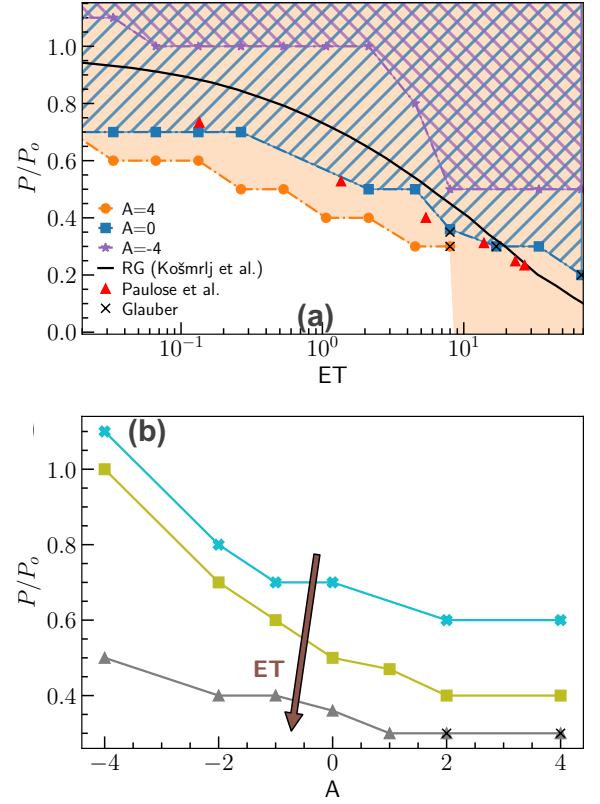


FIG. 3. **Phase diagram** The phase boundary in (a) the pressure–elasto–thermal number plane for different activities and (b) in the pressure–activity plane for different elasto–thermal numbers (gray triangles for $ET = 7.99$, olive squares for $ET = 2.12$ and cyan cross for $ET = 0.03$). In (a) the region where the buckled phase is obtained in equilibrium is marked by blue lines. The region where the buckled phase is obtained for $A = 4$ is shaded in light yellow. The region where the buckled phase is obtained for $A = -4$ is marked by violet lines. Cases marked with a cross uses the Glauber algorithm. In (a) the phase boundary obtained by RG calculation [31] is marked by a black line and the simulation results by Ref. [30] are represented by red triangles.

the results of Refs. [30, 31]. We show the results of the simulations for both the active, $A = 2$, and the sedate, $A = -2$ cases. For the former the critical buckling pressure decreases while for the latter the critical buckling pressure increases.

Next we decompose the fluctuating height field, $f(\theta, \phi)$ in spherical harmonics, $\mathcal{Y}_{\ell,m}(\theta, \phi)$:

$$f(\theta, \phi) = \sum_{\ell,m} \tilde{f}_{\ell,m} \mathcal{Y}_{\ell}^m(\theta, \phi), \quad \text{and define} \quad (6a)$$

$$S(\ell) = \frac{4\pi}{(2\ell+1)|\tilde{f}_{00}|^2} \sum_{m=-\ell}^{\ell} |\tilde{f}_{\ell,m}|^2 \quad (6b)$$

In supplementary material we compare typical plots of $S(\ell)$ for buckled and unbuckled shells. Buckling is accompanied by appearance of a peak in $S(\ell)$ at a small ℓ

value. For the equilibrium case, buckling as a function of external pressure is an equilibrium phase transition with the amplitude of the peak of $S(\ell)$ at small ℓ as the order parameter [30]. But buckling at the fixed P and ET as a function of activity is not an equilibrium phase transition but can be considered as a dynamical one. Nevertheless, we can still characterize buckling by appearance of a peak in $S(\ell)$ for small ℓ .

To obtain the phase diagram we use thirteen values of elasto-thermal number, for each of which we use seven values of activity. For a fixed choice of elasto-thermal number and activity we start our simulations with an initial condition where the shell is a perfect sphere. Then we choose a fixed value of external pressure and run our simulations till we reach a stationary state, which for zero activity is the equilibrium state. Whether the shell is buckled or not is decided by three checks: (a) significant decrease of volume (b) a peak at small ℓ for $S(\ell)$ (c) visual inspection. If the shell is not buckled we choose a higher external pressure and start our simulations again from the same initial condition. The buckling pressure, P_c obtained for a set of parameters is given in supplementary material. This way we mark out the phase boundary in the pressure-elasto-thermal number plane for different activities and in the pressure-activity plane for different elasto-thermal numbers, see Fig. (3). In Fig. (3a) we also plot the phase boundary, obtained through a RG calculation in Ref. [31], which agrees reasonably well with our numerical results for zero activity. Note that for large enough values of ET and A we reach a part of the phase diagram where the shell is unstable at zero external pressure and can be made stable only with positive internal pressure. This part of the phase diagram is not shown in Fig. (3) although the relevant data are included in supplementary material. Note that at small ET for the sedate case it is possible to have the shell remain unbuckled even for pressure higher P_0 , i.e., the shell is stabilized.

Several comments are now in order: One, most of our simulations use $N = 5120$. We have repeated some of our simulations with $N = 20252$ and obtained the same buckling pressure. Two, to obtain the buckling pressure we always start from the same initial condition and imposed a fixed external pressure. Hence, the lines of phase separation we show, Fig. (3), are not continuous and will be improved if the phase diagram is sampled in a finer resolution. Three, experimentally, it is unclear how to implement the sedate regime, negative A . Nevertheless, synthetic membranes that can be turned active ($A > 0$) optically, has been already realized by embedding certain proteins in a bi-lipid membranes – proteins that act as active pumps when irradiated with light of certain frequency [41, 42]. In such cases, only a fraction of points on the shell are active. This can be incorporated in a straightforward manner in our code and it would be interesting to see how the critical buckling pressure changes as we change the fraction of active points. Four, bi-lipid membranes are semi-permeable [61]. As the shell buckles the fraction of solute increases, increasing the partial

pressure inside the shell. Experimentally, this can be avoided by using shell with holes in them. We expect, in such cases the buckling pressure may change by a small amount. Five, as there are many different models of active elastic material it behooves us to study the universality of our result by performing similar simulations in other models. This is outside the scope of the present work.

Finally, our simulations point towards the intriguing possibility that within the right range of elastic parameters, a shell that is not buckled in thermal equilibrium can be buckled if turned optically active. Based on this, we suggest that it is possible to experimentally design microscopic elastic shells whose buckling can be optically controlled. In such devices it may be possible to drive flows at microscopic scales by buckling and unbuckling of shells, optically.

ACKNOWLEDGMENTS

We thank Apurba Dev, A. Fragkiadoulakis, Sreekanth M. Manikandan, Pinaki Chaudhuri and Bidisha Sinha for useful discussions. We gratefully acknowledge the use of the following free software packages: meshzoo [64, 65], matplotlib [66] and VisIt [67]. The simulations were performed on resources provided by the Swedish National Infrastructure for Computing (SNIC) at PDC center for high performance computing and the HPC facility supported by the Technical Division at the Department of Physics, Stockholm University. For the latter, we gratefully acknowledge generous help from Mikica Kocic. We acknowledge the financial support of the Swedish Research Council through grants 638-2013-9243 and 2016-05225.

CODE AND DATA AVAILABILITY

The source code used for the simulations of the study is freely available at <https://github.com/vipinagrawal25/MeMC/releases/tag/v1.1> [48]. The simulation setup and the corresponding data are freely available on Zenodo with DOI: 10.5281/zenodo.6772570. Python scripts are included with the data to generate all the figures.

Appendix A: Monte Carlo simulation of elastic shells in thermal equilibrium

We use a Monte Carlo algorithm following Refs. [30, 45] to study the elastic properties of shells. A version of our code, which performs thermal simulation of elastic shells, is already available as an open source software [48]. Here we describe the algorithm in brief and compare the results for elastic properties of shells in thermal equilibrium with those obtained in Ref. [30]. How we adapt the same

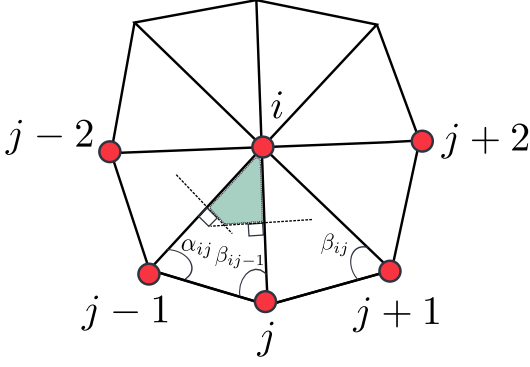


FIG. 4. An example of triangulated mesh at the node i . α_{ij}, β_{ij} are the angles opposite to the bond ij . Shaded part is the Voronoi region of triangle T at the nodes $i, j-1, j$ – it lies inside as T is non-obtuse. The nodes are sorted in counterclockwise direction. The image is adapted from Ref. [48].

algorithm to study shells out of equilibrium is described in the main body of this paper.

1. Algorithm

We start with N randomly chosen points on a sphere. Then, we run a Monte Carlo simulation, with a repulsive Lennard-Jones (LJ) potential, of these points moving on the surface of the sphere. Once the surface Monte Carlo (SMC) has reached thermal equilibrium, we triangulate the points using the algorithm described in Ref. [64]. This is our initial configuration. The distance between two neighboring nodes i and j is called ℓ_{ij}^0 .

We use Monte Carlo [25] simulations to update the positions of the points (\mathbf{X}_i at node i). For a pressurized shell, the total energy

$$E = E_{\text{stretch}} + E_{\text{bend}} + PV, \quad (\text{A1})$$

where the stretching and the bending contributions are, respectively,

$$E_{\text{stretch}} = \frac{1}{2} \sum_i \frac{H}{2} \sum_{j(i)} (\mathbf{X}_{ij} - \ell_{ij}^0)^2, \quad \text{where} \quad (\text{A2a})$$

$$X_{ij} \equiv |\mathbf{X}_i - \mathbf{X}_j| \quad \text{and} \quad (\text{A2b})$$

$$E_{\text{bend}} = \frac{B}{2} \sum_i \mathcal{A}_i (L_i - C\hat{\mathbf{n}})^2. \quad (\text{A2c})$$

Here P is the pressure difference between outside and inside the shell, and V is the volume. The Young's modulus of the membrane is given by $Y = 2H/\sqrt{3}$ [47]. The bending modulus is B , $\hat{\mathbf{n}}$ is the outward normal to the surface, C is its spontaneous curvature, and \mathcal{A}_i is the area of Voronoi dual cell at the node i [48, 62, 63]. The

operator

$$\mathbf{L}_i = \frac{1}{\mathcal{A}_i} \sum_{j(i)} \frac{1}{2} [\cot(\alpha_{ij}) + \cot(\beta_{ij})] \mathbf{X}_{ij}, \quad (\text{A3})$$

is the discrete Laplacian [47, 62, 63] at the node i . Here α_{ij}, β_{ij} are the angles opposite to bond \mathbf{X}_{ij} as shown in Fig. (4). We compute \mathcal{A}_i as follows [62, 63]. Consider the triangle T in Fig. (4), defined by the nodes $i, j, j-1$. If T is non-obtuse, the area of shaded region in Fig. (4) is

$$\mathcal{A}_{j(i)} = \frac{1}{8} [X_{ij}^2 \cot(\alpha_{ij}) + X_{ij-1}^2 \cot(\beta_{ij-1})]. \quad (\text{A4})$$

If T is an obtuse triangle, the shaded region in Fig. (4) lies outside the triangle T , then if the angle at the vertex i of T is obtuse $\mathcal{A}_{j(i)} = \text{area}(T)/2$ otherwise $\mathcal{A}_{j(i)} = \text{area}(T)/4$. Here $\text{area}(T) = (1/2)|\mathbf{X}_{ij} \times \mathbf{X}_{ij-1}|$. The area \mathcal{A}_i is obtained by summing up the contributions from all the triangles similar to $\mathcal{A}_{j(i)}$, in Fig. (4), e.g., the contribution from the triangle T is the shaded area.

To compute the outward normal to the surface, $\hat{\mathbf{n}}$, in Eq. (A2c), we sort the points about node i in a counterclockwise manner. To sort the neighbors around any node i , we rotate the coordinate system such that, the z axis passes through the point i along the vector \mathbf{X}_i . In this coordinate system we sort the neighbors by their azimuthal angle. Note that unlike Ref. [45] we do not incorporate self-avoidance.

2. Comparison with Paulose et al. [30]

We use the radius of the sphere $R = 1$ as our unit of length and $k_B T = 1$ as our unit of energy.

We decompose the fluctuating height field, $f(\theta, \phi)$ in spherical harmonics, $\mathcal{Y}_\ell^m(\theta, \phi)$:

$$f(\theta, \phi) = \sum_{\ell, m} \tilde{f}_{\ell, m} \mathcal{Y}_\ell^m(\theta, \phi), \quad \text{and define} \quad (\text{A5a})$$

$$S(\ell) \equiv \frac{4\pi}{(2\ell+1)|\tilde{f}_{00}|^2} \sum_{m=-\ell}^{\ell} |\tilde{f}_{\ell, m}|^2. \quad (\text{A5b})$$

In Fig. (5) we plot the spectra $S(\ell)$ for number of nodes $N = 20252$, the Föppl-von-Karman number $\text{FvK} \equiv YR^2/B = 4616$ and for three values of the bending rigidity, $k_B T/B = 7 \times 10^{-4}$ (blue), 0.07 (red) and 0.18 (orange). The continuous line shows the theoretical prediction by Ref. [30] the shaded region is the error obtained by using BAGGING (B1) – we find reasonable agreement with the theory. Next, following Ref. [30] we measure the mechanical response of a thermal shell by deforming it equally at the two poles with two point-like indentations. This is implemented by two harmonic springs that are attached to the north and the south poles of the shell. In Fig. (5B) we compare the force-deformation curve from

Parameters	our simulation	Ref. [30]
Number of grid points, N	5120 to 20252	5530 to 41816
Activity, A	-4 to 4	0
P/P_0	-4 to 1	0.2 to 1
Elasto thermal number, ET	1.65×10^{-2} to 68	10^{-6} to 10^2
Föppl-von Kármán, FvK	4616	650 to 35000
Total MC steps	$10^6 - 5 \times 10^7$	1.25×10^8

TABLE I. Comparison between our simulations and those in Ref. [30].

our simulations with those obtained in Ref. [30]. Again we obtain quite reasonable agreement. A detailed comparison of parameters of our simulations with those of Ref. [30] is given in Table I.

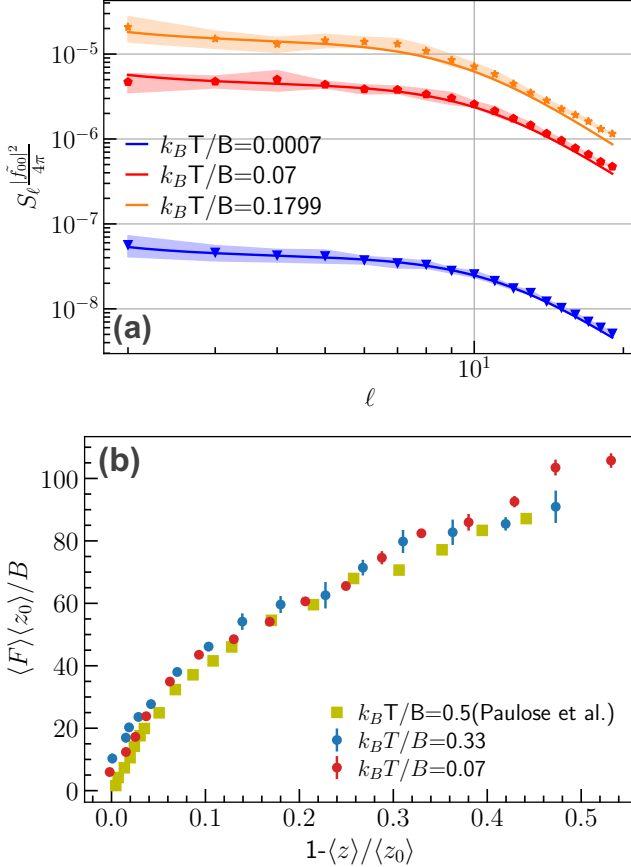


FIG. 5. **Comparison with Ref Paulose *et al.* [30]:** (a) The fluctuation spectrum $S(\ell)$ versus ℓ for different values of bending modulus B . The solid lines are theoretical predictions [30]. The lines with symbols are from our simulations. The shaded area shows the error, see section (B 1). (b) The force-deformation curve from our simulations compared with Ref. [30] (yellow squares). We use $N = 20292$ and FvK = 4616.

3. Comparison between Glauber and Metropolis algorithm

We run Monte Carlo simulations with both Metropolis (W_{Met}) and the Glauber (W_{Gla}), rates:

$$W_{\text{Met}} = \min \left[1, \exp \left(-\frac{E}{k_B T} \right) \right] \text{ and} \quad (\text{A6a})$$

$$W_{\text{Gla}} = \frac{1}{2} \left[1 - \tanh \left(\frac{E}{2k_B T} \right) \right]. \quad (\text{A6b})$$

Here k_B is the Boltzmann constant, T is the temperature and E is the difference in energy between the two states. In Fig. (6), we compare the probability distribution function (PDF) of the energy (in thermal equilibrium) of individual nodes obtained by the Glauber and the Metropolis rules. As expected, the PDF shows the same Boltzmann distribution in both cases.

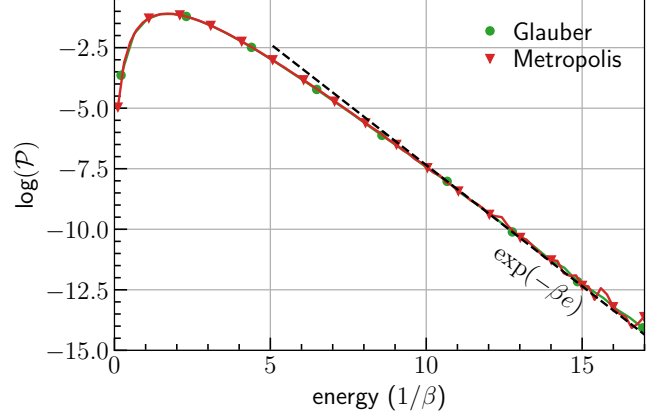


FIG. 6. **Probability distribution function** of energy at each point of the surface for Glauber and Metropolis algorithm for $N=20252$, and total MC steps = 10^6 .

Appendix B: Monte Carlo simulations out of equilibrium

To drive the membrane out of equilibrium, following Ref. [44], we replace E in (A6) by $E + \Delta E$ where ΔE is a constant. This guarantees that detailed balance is broken and the amount by which it is broken is ΔE . If ΔE is positive (negative) the probability of acceptance of large fluctuations is decreased (increased). Thus we define a dimensionless quantity $A = -\Delta E/(k_B T)$ such that simulations with positive A , *active* simulations, have higher fluctuations than equilibrium ones whereas for negative A , *sedate* simulations, the fluctuations are less than the equilibrium ones. A complete list of parameters are shown in caption of table (II).

In Fig. (7) we plot the probability distribution function (PDF) of energy of individual nodes. For the equilibrium case the tail of the PDF can be fitted with

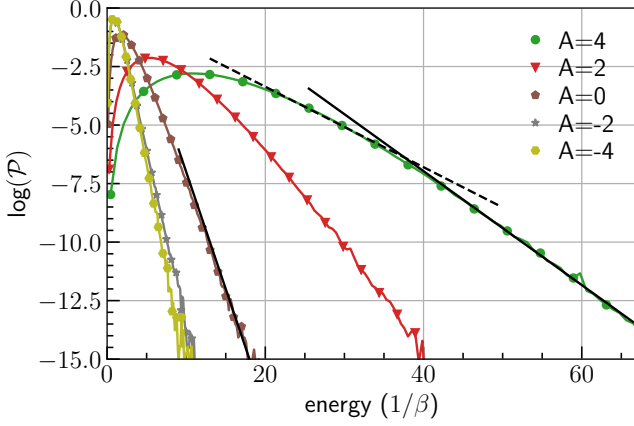


FIG. 7. **Probability distribution function** of energies of every node in the stationary state for activity $A = -4, -2, 0, 2, 4$. The distribution fits an exponential distribution for the thermal ($A=0$) case. However for the active case (e.g. $A=4$), the distribution does not fit single exponential curve.

$\mathcal{P}(E) \sim \exp(-(E/k_B T))$, where E is the energy of a node. But for the out-of-equilibrium cases there is no one exponential that can be used to fit. The fluctuation spectrum $S(\ell)$ comparing unbuckled and buckled simulations are shown in Fig. (8). The unbuckled ones, even when out of equilibrium, shows $S(\ell) \sim \ell^{-4}$ for a range of scales. The buckled ones show distinctive peak at small values of ℓ .

To obtain the phase diagram we use thirteen values of elasto-thermal number, for each of which we use seven values of activity. For a fixed choice of elasto-thermal number and activity we start our simulations with an initial condition where the shell is a perfect sphere. Then we choose a fixed value of external pressure and run our simulations till we reach a stationary state, which for zero activity is the equilibrium state. Whether the shell is buckled or not is decided by three checks: (a) significant decrease of volume (b) a peak at small ℓ for $S(\ell)$ (c) visual inspection. If the shell is not buckled we choose a higher external pressure and start our simulations again from the same initial condition. The buckling pressure, P_c obtained for a set of parameters is given in table (II). This way we mark out the phase boundary in the pressure-elasto-thermal number plane for different activities and in the pressure-activity plane for different elasto-thermal numbers, see Fig. 3 in main text. In the Fig. 3(a) of the main text, we also plot the phase boundary, obtained through a RG calculation in Ref. [31], which agrees reasonably well with our numerical results for zero activity. Note that for large enough values of ET and A we reach a part of the phase diagram where the shell is unstable at zero external pressure and can be made stable only

with positive internal pressure. This part of the phase diagram is not shown, although the relevant data are included in table (II). Note that at small ET for the sedate case it is possible to have the shell remain unbuckled even

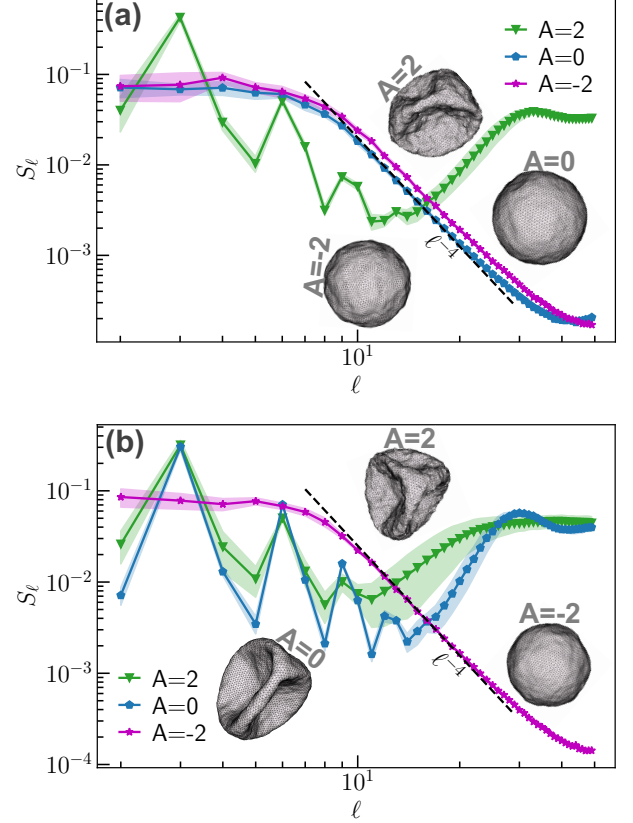


FIG. 8. **Spectra:** The spectra, $S(\ell)$, ($A5$), $\ell \geq 2$ and (a) $P = 0.3P_0$ and (b) $P = 0.36P_0$ for thermal (blue) active (green, $A = 2$) and sedate (magenta, $A = -2$). The solid lines are the mean of spectra and shaded regions are the error. Appearance of a peak at small ℓ signifies buckling.

for pressure higher P_0 , i.e., the shell is stabilized.

1. Estimation of error

To compute the statistical error in a dataset Ψ , we partition it into M smaller datasets $\{\Psi_1, \dots, \Psi_M\}$. Then for each partition we calculate the statistical quantities, e.g., mean, spectrum, etc. The average over the partitions is the average value we quote and the error is the standard deviation calculated across the partitions. We use $M = 10$. This technique is called BAGging or Bootstrap AGGregation [46].

[1] There are several geodesic domes with sizes ranging from 10 to 200 meters.

[2] Mathias Buenemann and Peter Lenz, “Elastic properties and mechanical stability of chiral and filled viral capsids,”

$\frac{A}{E\Gamma}$	4	2	1	0	-1	-2	-4
1.65×10^{-2}	0.70	0.70	—	0.70	0.70	0.80	1.10
3.32×10^{-2}	0.60	0.60	—	0.70	0.70	0.80	1.10
6.63×10^{-2}	0.60	0.60	0.60	0.70	0.70	0.80	1.00
1.33×10^{-1}	0.60	0.60	0.60	0.70	0.70	0.80	1.00
2.65×10^{-1}	0.50	0.60	0.60	0.70	0.70	0.80	1.00
5.31×10^{-1}	0.50	0.50	0.60	—	0.70	0.80	1.00
1.06	0.40	0.40	0.50	—	0.60	0.80	1.00
2.12	0.40	0.40	0.47	0.50	0.60	0.70	1.00
4.53	0.30	0.30	—	0.50	0.50	0.60	0.80
7.99	<u>0.30</u>	<u>0.30</u>	0.30	0.36	0.40	0.40	0.50
16.99	-2.8	—	—	0.30	0.40	0.40	—
33.97	<-4	-2.5	—	0.30	0.30	0.40	0.50
67.94	<-4	<-4	-0.10	<u>0.20</u>	0.30	0.30	0.50

TABLE II. **Buckling pressure**(P_c/P_0): for different values of elasto-thermal number ($E\Gamma$) and activity (A) obtained from the simulation with $FvK=4616$, $N = 5120$, $R = 1$ and $k_B T = 1$, where N is the number of grid points, R is radius of the shell, k_B is the Boltzmann constant and T is the temperature. We repeated some of the simulations for $N = 20252$ and obtained the same buckling pressure. To reach a stationary state, typically, we need to run for $10^6 - 5 \times 10^7$ Monte Carlo steps, where in one Monte Carlo step, we perform $2N$ Monte Carlo iterations to attempt to update the position a random point. Underlined values have been reproduced with Glauber algorithm as well.

Physical Review E **78**, 051924 (2008).

- [3] JP Michel, IL Ivanovska, MM Gibbons, WS Klug, CM Knobler, GJL Wuite, and CF Schmidt, “Nanoin-indentation studies of full and empty viral capsids and the effects of capsid protein mutations on elasticity and strength,” *Proceedings of the National Academy of Sciences* **103**, 6184–6189 (2006).
- [4] D Michiel Pegtel and Stephen J Gould, “Exosomes,” *Annual review of biochemistry* **88**, 487–514 (2019).
- [5] Sara Cavallaro, Josef Horak, Petra Haag, Dhanu Gupta, Christiane Stiller, Siddharth S Sahu, Andre Gorgens, Hithesh K Gatty, Kristina Viktorsson, Samir El Andaloussi, *et al.*, “Label-free surface protein profiling of extracellular vesicles by an electrokinetic sensor,” *ACS sensors* **4**, 1399–1408 (2019).
- [6] Augustus Edward Hough Love, *A treatise on the mathematical theory of elasticity* (Dover Publications; 4th edition, 2011).
- [7] LD Landau and EM Lifshitz, *Theory of Elasticity*, Course of Theoretical Physics, Vol. 7 (Pergamon Press Ltd., Oxford, England, 1970).
- [8] WT Koiter, “Progress in applied mechanics (the prager anniversary volume),” (1963).
- [9] Koiter WT, “Current trends in theory of buckling,” in *Buckling of structures: Symposium Cambridge/USA*, edited by Bernard Budiansky (Springer-Verlag, Berlin, Heidelberg, New York, 1976) pp. 1–16.
- [10] Alekse Vasilevich Pogorelov, *Bendings of surfaces and stability of shells*, Vol. 72 (American Mathematical Soc., 1988).
- [11] John W Hutchinson, “Buckling of spherical shells revisited,” *Proceedings of the Royal Society A: Mathematical, Physical and Engineering Sciences* **472**, 20160577 (2016).
- [12] Gerard Adriaan Vliegenthart and Gerhard Gompper, “Mechanical deformation of spherical viruses with icosahedral symmetry,” *Biophysical journal* **91**, 834–841 (2006).
- [13] Ch Gao, E Donath, S Moya, V Dudnik, and H Möhwald, “Elasticity of hollow polyelectrolyte capsules prepared by the layer-by-layer technique,” *The European Physical Journal E* **5**, 21–27 (2001).
- [14] Vernita D Gordon, Xi Chen, John W Hutchinson, Andreas R Bausch, Manuel Marquez, and David A Weitz, “Self-assembled polymer membrane capsules inflated by osmotic pressure,” *Journal of the American Chemical Society* **126**, 14117–14122 (2004).
- [15] Dominic Vella, Amin Ajdari, Ashkan Vaziri, and Arezki Boudaoud, “The indentation of pressurized elastic shells: from polymeric capsules to yeast cells,” *Journal of the Royal Society Interface* **9**, 448–455 (2012).
- [16] Daan Vorselen, Fred C MacKintosh, Wouter H Roos, and Gijs JL Wuite, “Competition between bending and internal pressure governs the mechanics of fluid nanovesicles,” *Acs Nano* **11**, 2628–2636 (2017).
- [17] Pei-Hsun Wu, Dikla Raz-Ben Aroush, Atef Asnacios, Wei-Chiang Chen, Maxim E Dokukin, Bryant L Doss, Pauline Durand-Smet, Andrew Ekpenyong, Jochen Guck, Natalia V Guz, *et al.*, “A comparison of methods to assess cell mechanical properties,” *Nature methods* **15**, 491–498 (2018).
- [18] Daan Vorselen, Melissa C Piontek, Wouter H Roos, and Gijs JL Wuite, “Mechanical characterization of liposomes and extracellular vesicles, a protocol,” *Frontiers in molecular biosciences* **7**, 139 (2020).
- [19] Sara Cavallaro, Federico Pevere, Fredrik Stridfeldt, André Görgens, Carolina Paba, Siddharth S Sahu, Doste R Mamand, Dhanu Gupta, Samir El Andaloussi, Jan Linnros, *et al.*, “Multiparametric profiling of single nanoscale extracellular vesicles by combined atomic force and fluorescence microscopy: correlation and heterogeneity in their molecular and biophysical features,” *Small* **17**, 2008155 (2021).
- [20] CI Zoldesi, IL Ivanovska, C Quilliet, GJL Wuite, and A Imhof, “Elastic properties of hollow colloidal particles,” *Physical Review E* **78**, 051401 (2008).
- [21] Jonathan A Jackson, Nicolas Romeo, Alexander Mietke, Keaton J Burns, Jan F Totz, Adam C Martin, Jörn Dunkel, and Jasmin Imran Alsous, “Dynamics, scaling behavior, and control of nuclear wrinkling,” *arXiv preprint arXiv:2210.11581* (2022).
- [22] Gerald Lim HW, Michael Wortis, and Ranjan Mukhopadhyay, “Stomatocyte–discocyte–echinocyte sequence of the human red blood cell: Evidence for the bilayer–couple hypothesis from membrane mechanics,” *Proceedings of the National Academy of Sciences* **99**, 16766–16769 (2002).
- [23] Dmitry A Fedosov, Bruce Caswell, and George Em Karniadakis, “A multiscale red blood cell model with accurate mechanics, rheology, and dynamics,” *Biophysical journal* **98**, 2215–2225 (2010).
- [24] Dmitry A Fedosov, Bruce Caswell, and George Em Karniadakis, “Systematic coarse-graining of spectrin-level red blood cell models,” *Computer Methods in Applied Mechanics and Engineering* **199**, 1937–1948 (2010).
- [25] Dmitry A Fedosov, Bruce Caswell, and George Em Karniadakis, “Systematic coarse-graining of spectrin-level red blood cell models,” *Computer Methods in Applied*

- Mechanics and Engineering **199**, 1937–1948 (2010).
- [26] Dmitry A Fedosov, *Multiscale modeling of blood flow and soft matter*, Ph.D. thesis, Division of Applied Mathematics at Brown University (2010).
- [27] Dmitry A Fedosov, Wenxiao Pan, Bruce Caswell, Gerhard Gompper, and George E Karniadakis, “Predicting human blood viscosity in silico,” *Proceedings of the National Academy of Sciences* **108**, 11772–11777 (2011).
- [28] Jonathan B Freund, “Numerical simulation of flowing blood cells,” *Annual review of fluid mechanics* **46**, 67–95 (2014).
- [29] Lailai Zhu, Cecilia Rorai, Dhrubaditya Mitra, and Luca Brandt, “A microfluidic device to sort capsules by deformability: a numerical study,” *Soft Matter* **10**, 7705–7711 (2014).
- [30] Jayson Paulose, Gerard A Vliegenthart, Gerhard Gompper, and David R Nelson, “Fluctuating shells under pressure,” *Proceedings of the National Academy of Sciences* **109**, 19551–19556 (2012).
- [31] Andrej Košmrlj and David R Nelson, “Statistical mechanics of thin spherical shells,” *Physical Review X* **7**, 011002 (2017).
- [32] Erwin Schrödinger, *What is life?: With mind and matter and autobiographical sketches* (Cambridge university press, 2012).
- [33] F S Gnesotto, F Mura, J Gladrow, and C P Broedersz, “Broken detailed balance and non-equilibrium dynamics in living systems: a review,” *Reports on Progress in Physics* **81**, 066601 (2018).
- [34] M Cristina Marchetti, Jean-François Joanny, Sriram Ramaswamy, Tanniemola B Liverpool, Jacques Prost, Madan Rao, and R Aditi Simha, “Hydrodynamics of soft active matter,” *Reviews of modern physics* **85**, 1143 (2013).
- [35] Sriram Ramaswamy, “The mechanics and statistics of active matter,” *The Annual Review of Condensed Matter Physics* **1**, 323–45 (2010).
- [36] Zhangli Peng, Xuejin Li, Igor V Pivkin, Ming Dao, George E Karniadakis, and Subra Suresh, “Lipid bilayer and cytoskeletal interactions in a red blood cell,” *Proceedings of the National Academy of Sciences* **110**, 13356–13361 (2013).
- [37] Hervé Turlier, Dmitry A Fedosov, Basile Audoly, Thorsten Auth, Nir S Gov, Cécile Sykes, J-F Joanny, Gerhard Gompper, and Timo Betz, “Equilibrium physics breakdown reveals the active nature of red blood cell flickering,” *Nature physics* **12**, 513–519 (2016).
- [38] Arikta Biswas, Amal Alex, and Bidisha Sinha, “Mapping cell membrane fluctuations reveals their active regulation and transient heterogeneities,” *Biophysical journal* **113**, 1768–1781 (2017).
- [39] Hervé Turlier and Timo Betz, “Unveiling the active nature of living-membrane fluctuations and mechanics,” *Annual Review of Condensed Matter Physics* **10**, 213–232 (2019).
- [40] Sreekanth K Manikandan, Tanmoy Ghosh, Tithi Mandal, Arikta Biswas, Bidisha Sinha, and Dhrubaditya Mitra, “Estimate of entropy generation rate can spatiotemporally resolve the active nature of cell flickering,” *arXiv preprint arXiv:2205.12849* (2022).
- [41] P Girard, J Prost, and P Bassereau, “Passive or active fluctuations in membranes containing proteins,” *Physical review letters* **94**, 088102 (2005).
- [42] J-B Manneville, P Bassereau, S Ramaswamy, and J Prost, “Active membrane fluctuations studied by micropipet aspiration,” *Physical Review E* **64**, 021908 (2001).
- [43] Dong Yan, Matteo Pezzulla, Lilian Cruveiller, Arefeh Abbasi, and Pedro M Reis, “Magneto-active elastic shells with tunable buckling strength,” *Nature communications* **12**, 1–9 (2021).
- [44] Manoj Kumar and Chandan Dasgupta, “Nonequilibrium phase transition in an ising model without detailed balance,” *Physical Review E* **102**, 052111 (2020).
- [45] G Gompper and DM Kroll, “Triangulated-surface models of fluctuating membranes,” in *Statistical mechanics of membranes and surfaces*, edited by David Nelson, Tsvi Piran, and Steven Weinberg (World Scientific, 2004) pp. 359–426.
- [46] Pankaj Mehta, Marin Bukov, Ching-Hao Wang, Alexandre GR Day, Clint Richardson, Charles K Fisher, and David J Schwab, “A high-bias, low-variance introduction to machine learning for physicists,” *Physics reports* **810**, 1–124 (2019).
- [47] C Itzykson, in *Proceedings of the GIFT seminar, Jaca 85*, edited by J et al Abad (World Scientific Singapore, 1986) pp. 130–188.
- [48] Vipin Agrawal, Vikash Pandey, Hanna Kylhammar, Apurba Dev, and Dhrubaditya Mitra, “Memc: A package for monte carlo simulations of spherical shells,” *Journal of Open Source Software* **7**, 4305 (2022).
- [49] Sriram Ramaswamy, John Toner, and Jacques Prost, “Nonequilibrium fluctuations, traveling waves, and instabilities in active membranes,” *Physical review letters* **84**, 3494 (2000).
- [50] Madan Rao and Sarasij R.C., “Active fusion and fission processes on a fluid membrane,” *Physical review letters* **87**, 128101 (2001).
- [51] Bastien Loubet, Udo Seifert, and Michael Andersen Lomholt, “Effective tension and fluctuations in active membranes,” *Physical Review E* **85**, 031913 (2012).
- [52] Ananyo Maitra, Pragma Srivastava, Madan Rao, and Sriram Ramaswamy, “Activating membranes,” *Physical review letters* **112**, 258101 (2014).
- [53] Rhoda J Hawkins and Tanniemola B Liverpool, “Stress reorganization and response in active solids,” *Physical review letters* **113**, 028102 (2014).
- [54] Sifan Yin, Bo Li, and Xi-Qiao Feng, “Bio-chemomechanical theory of active shells,” *Journal of the Mechanics and Physics of Solids* **152**, 104419 (2021).
- [55] A Goriely, “Five ways to model active processes in elastic solids: active forces, active stresses, active strains, active fibers, and active metrics,” *Mech. Res. Commun* **93**, 75–79 (2017).
- [56] H Künsch, “Non reversible stationary measures for infinite interacting particle systems,” *Zeitschrift für Wahrscheinlichkeitstheorie und Verwandte Gebiete* **66**, 407–424 (1984).
- [57] Claude Godreche and Alan J Bray, “Nonequilibrium stationary states and phase transitions in directed ising models,” *Journal of Statistical Mechanics: Theory and Experiment* **2009**, P12016 (2009).
- [58] Claude Godrèche, “Rates for irreversible gibbsian ising models,” *Journal of Statistical Mechanics: Theory and Experiment* **2013**, P05011 (2013).
- [59] J Prost and R Bruinsma, “Shape fluctuations of active membranes,” *EPL (Europhysics Letters)* **33**, 321 (1996).

- [60] A. Fragkiadoulakis, S.K. Manikandan, and D. Mitra, unpublished.
- [61] Rob Phillips, Jane Kondev, Julie Theriot, Hernan G Garcia, and Nigel Orme, *Physical biology of the cell* (Garland Science, 2012).
- [62] Mark Meyer, Mathieu Desbrun, Peter Schröder, and Alan H Barr, “Discrete differential-geometry operators for triangulated 2-manifolds,” in *Visualization and mathematics III* (Springer, 2003) pp. 35–57.
- [63] Hans-Christian Hege and Konrad Polthier, *Visualization and mathematics III* (Springer Science & Business Media, 2003).
- [64] Manuel Caroli, Pedro MM de Castro, Sébastien Lorient, Olivier Rouiller, Monique Teillaud, and Camille Wormser, “Robust and efficient delaunay triangulations of points on or close to a sphere,” in *International Symposium on Experimental Algorithms* (Springer, 2010) pp. 462–473.
- [65] A simple and fast mesh generator, <https://github.com/meshpro/meshzoo>.
- [66] J. D. Hunter, “Matplotlib: A 2d graphics environment,” *Computing in Science & Engineering* **9**, 90–95 (2007).
- [67] Hank Childs, Eric Brugger, Brad Whitlock, Jeremy Meredith, Sean Ahern, David Pugmire, Kathleen Biagas, Mark Miller, Cyrus Harrison, Gunther H. Weber, Hari Krishnan, Thomas Fogal, Allen Sanderson, Christoph Garth, E. Wes Bethel, David Camp, Oliver Rübel, Marc Durant, Jean M. Favre, and Paul Navrátil, “VisIt: An End-User Tool For Visualizing and Analyzing Very Large Data,” in *High Performance Visualization—Enabling Extreme-Scale Scientific Insight* (2012) pp. 357–372.